JOURNAL OF MATERIALS SCIENCE 12 (1977) 1845–1852

# The strength of acrylic bone cements and acrylic cement-stainless steel interfaces

## Part 1 *The strength of acrylic bone cement containing second phase dispersions*

PETER W. R. BEAUMONT
*Department of Engineering, University of Cambridge, Cambridge, UK*

The strength and fracture toughness of a surgical acrylic bone cement have been evaluated in air, saline solution, and a blood serum, and little effect of environment was observed. Second phase dispersions of either barium sulphate or glass spheres were found to have significant effects upon the strength and fracture surface energy. In the first composite, a decrease in strength and fracture surface energy may be explained in terms of the formation of voids around the barium sulphate particles and tearing of material between them; in the second composite, an increase in strength and fracture surface energy occurred through a crack front–glass sphere interaction effect. The occurrence of sub-critical crack growth in the acrylic bone cement composites was investigated, and crack velocity–stress intensity factor diagrams were constructed for the purposes of fracture-safe design.

## 1. Introduction

A greater understanding of the mechanical behaviour of materials combined with improvements in surgical techniques has resulted in their wider use for the structural replacement of diseased and injured parts of the human skeleton. At first, failures occurred as the result of a poor appreciation of basic material properties; for example, in total hip joint replacement, some of the early non-clinical failures were due to excessive wear of polytetrafluorethylene selected for the acetabular cup. The outcome was a proliferation of dislocations of the hip prosthesis. More recently, the use of stainless steels and cobalt–chromium alloys for the femoral prosthesis together with high molecular weight polyethylene for the acetabular cup has essentially overcome the problem of unacceptable wear; and the use of self-curing acrylic polymers based upon polymethylmethacrylate (PMMA) as a filler or packing material between femoral stem and medullary canal has reduced the tendency for loosening and slippage of the hip prosthesis. The apparent success of acrylic bone "cement" for "anchoring" prosthetic devices is, however, despite its low ductility and inherent brittleness, although the problem of femoral stem loosening still persists. There is some evidence to link this loosening of the femoral stem with cracking in the acrylic "cement"; and to connect fracture of the metallic stem with failure at the metal–polymer interface [1].

In many of the surgical acrylic bone "cements" currently available are dispersions of barium sulphate ($BaSO_4$) particles in small amounts ($\sim 3$ vol%). The presence of $BaSO_4$ renders the acrylic material radiopaque and therefore more useful to the orthopaedic surgeon from a clinical point of view. But the questions which remain unanswered include "how does the dispersion of $BaSO_4$ powder affect the strength and fracture toughness of the acrylic *cement;* and how does the presence of a physiological environment, for example, blood or saline solution, affect the mechanical and fracture properties of the *cement* and *cement*–metal interface?"

© *1977 Chapman and Hall Ltd. Printed in Great Britain.*

This paper is divided into 2 parts; Part 1 describes a study into the effects of $BaSO_4$ inclusions upon the plane-strain fracture toughness, $K_{IC}$, and fracture surface energy, $\Gamma_C$, of a surgical acrylic bone *cement* based on PMMA*. Any occurrence of subcritical (slow) crack growth in the acrylic material was investigated as a function of $BaSO_4$ content using a linear elastic fracture mechanics approach. The effects of a saline solution and a blood serum upon the fracture behaviour were also evaluated. The fracture properties of a modified acrylic bone *cement* based upon Simplex P and containing a dispersion of microscopical glass spheres are described also in terms of $K_{IC}$, $\Gamma_c$, and crack velocity ($V$)–crack tip stress intensity factor ($K_I$) relationships.

Part 2 describes the use of a shear lag model to explain the effects of a blood serum upon the shear strength and shear modulus of a stainless steel–acrylic bone *cement* interface. The shear strength of the metal–polymer interface is then compared to a theoretical estimation of the interfacial shear stresses that act at a femoral prosthesis–acrylic bone *cement* interface in a total hip joint replacement.

## 2. Materials

A surgical acrylic bone *cement* based upon PMMA (Simplex P) has been used as a matrix material in two particulate composites. In one composite were dispersed particles of $BaSO_4$ which have a mean diameter, $\bar{d}$, of 0.9 $\mu$m. It was fabricated by thoroughly mixing a known amount of $BaSO_4$ particles with PMMA powder; liquid methyl methacrylate (MMA) was then added to the mixture in the ratio 2 parts PMMA: 1 part MMA (by weight). When the resulting dough had lost its tackiness, (which took a few minutes only), it was placed between two mild steel plates and compressed to a thickness of 2 mm. Polymerization of the acrylic composite was essentially complete a few minutes later. Five samples were fabricated with increasing amounts of $BaSO_4$, added in increments of 1.5 vol %, up to a maximum of 6.0 vol % or 20 wt %.

A second composite was made using Simplex P powder (without $BaSO_4$) and glass spheres which have a mean diameter $\bar{d}$ of 75 $\mu$m. The glass spheres were thoroughly mixed with the PMMA powder before the liquid MMA monomer was added, and the composite was then fabricated using the same procedure as before. Five samples were made and they contained volume fractions of glass between 0 and 0.30.

## 3. Test procedure and analysis

Double-torsion (DT) specimens were machined from each composite. A detailed description of specimen geometry and experimental technique has been presented in [2, 3]. Briefly, a crack is introduced at one end of a rectangular plate which is then forced to propagate along the length of the specimen by loading the end containing the crack in 4-point bending. It can be shown that the stress intensity factor, $K_I$, associated with the crack tip is independent of crack length and is given by [3]

$$K_I = AP \qquad (1)$$

where $P$ is applied load and $A$ is a geometrical constant.

In a fixed displacement test, $(dy/dt = 0)$, the crack growth rate $(da/dt)_y$ is proportional to the rate of load relaxation $(dP/dt)_y$;

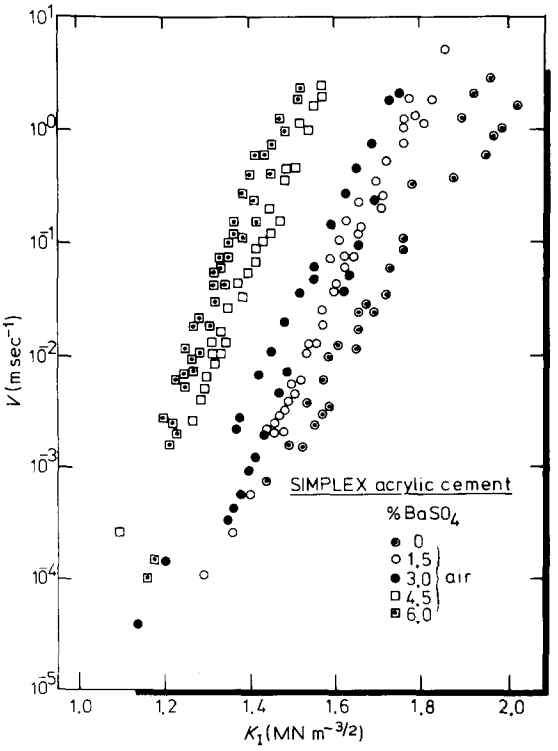


*Figure 1* $V(K_I)$ diagram for acrylic bone *cement* containing different volume fractions of $BaSO_4$ dispersions. (The data was collected in air at 20° (± 2°) C).

*The acrylic bone *cement* was Simplex P supplied by Howmedica Inc.

$$\left(\frac{da}{dt}\right)_y = V = -(P_{i,f}/P^2)\left(a_{i,f} + \frac{C}{B}\right)\left(\frac{dP}{dt}\right)_y \quad (2)$$

where $P_{i,f}$ is the initial (or final) load, $a_{i,f}$ is the initial (or final) crack size, and $C$ and $B$ are values of gradient and intercept, respectively, of a compliance, $(y/P)$, crack size $(a)$, calibration curve.

If the DT specimen is held at constant load ($dP/dt = 0$), the crack velocity, $V$, can be determined by measuring the initial and final values of crack length $a_{i,f}$ and the corresponding increment of time, $\Delta t$:

$$V = (a_f - a_i)/\Delta t \quad (3)$$

The value of $K_I$ associated with a moving crack of velocity $V$ can be determined by inserting the appropriate value of $P$ into Equation 1. This approach provides a check on the load relaxation technique.

## 4. Results and discussion

### 4.1. Effect of $BaSO_4$ particles

The relationship between crack velocity $V$ and stress intensity factor $K_I$ is shown in Fig. 1 in the form of a $V(K_I)$ diagram. Two principle effects of the $BaSO_4$ particles upon the rate of slow crack growth can be seen; (1) an increase in particle volume fraction, $V_p$, results in an increase in crack velocity, $V$, for a given value of $K_I$, and (2) the slope $n$ of the $V(K_I)$ curve increases from $n = 24$ for the unfilled acrylic *cement* to $n = 28$ for a composite containing 6 vol% $BaSO_4$.

If the curves are extrapolated to very slow crack velocities, they appear to intersect one another at a $K_I$ value of 0.8 MN m$^{-3/2}$ and a crack velocity of $10^{-9}$ m sec$^{-1}$ approximately. The $K_I$ value of 0.8 MN m$^{-3/2}$ is similar to the threshold value of $K_I$ measured for perspex [2], below which no cracking could be detected.

It was found impossible to separate to any significant extent the data collected in air from the data obtained from tests carried out in either saline solution or blood serum at 20° (± 2°)C (Figs. 2, 3 and 4).

Fig. 5 shows the effect of $BaSO_4$ upon the plane-strain fracture toughness, $K_{IC}$, and the fracture surface energy, $\Gamma_c$. These basic material parameters have decreased in value by about 40% and 25%, respectively, due to the addition of about 6 vol% $BaSO_4$. The Young's modulus $E$

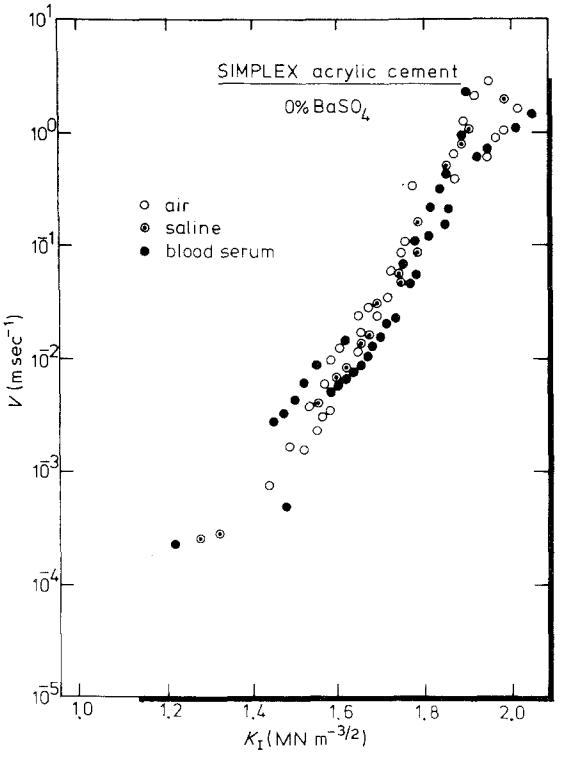


*Figure 2* $V(K_I)$ diagram for acrylic bone *cement* without a second phase dispersion. (The data was collected in air, saline solution and blood serum at 20° (± 2°) C).

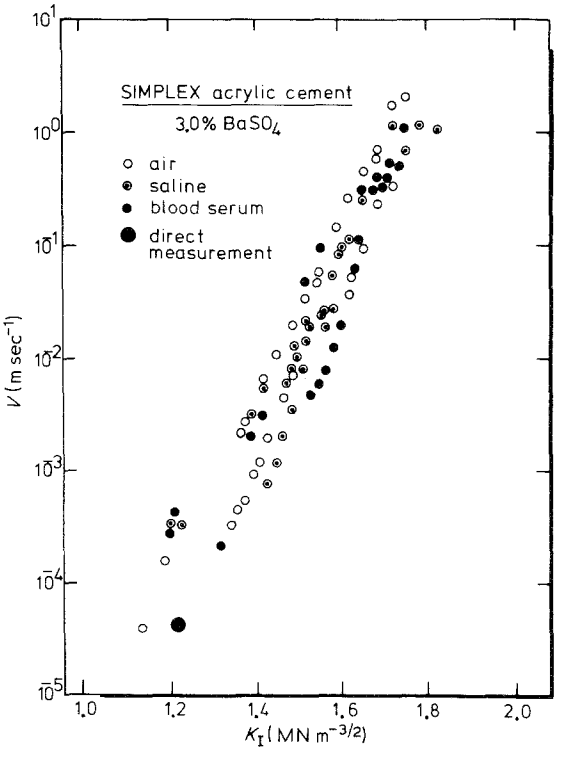


*Figure 3* $V(K_I)$ diagram for acrylic bone *cement* containing 3 vol% $BaSO_4$. (The data was collected in air, saline solution and blood serum at 20° (± 2°) C).

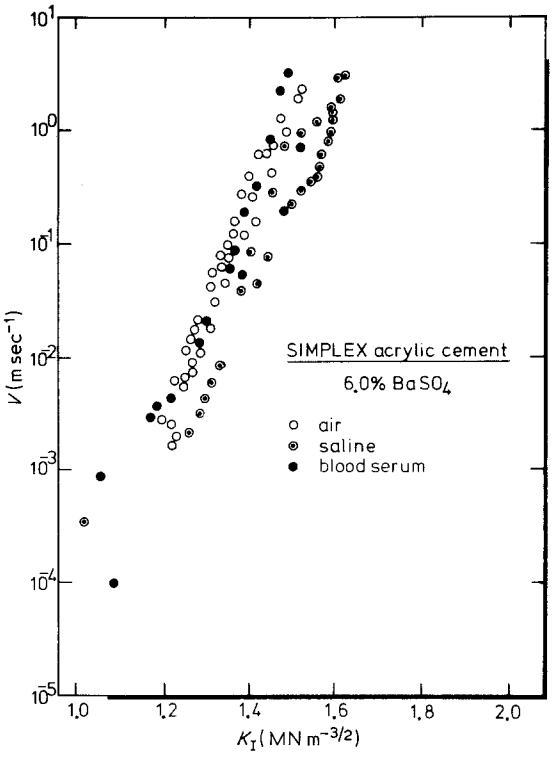


*Figure 4* $V(K_I)$ diagram for acrylic bone *cement* containing 6 vol% $BaSO_4$. (The data was collected in air, saline solution and blood serum at 20° (± 2°) C).

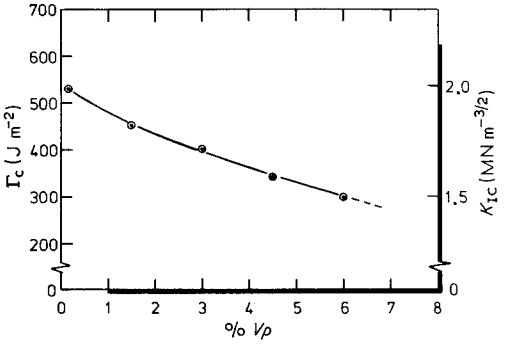


*Figure 5* $V(K_I)$ diagram for acrylic bone *cement* containing different volume fractions of glass spheres. (The data was collected in air at 20° (± 2°) C).

measured in a 3-point bend test, was essentially unaffected by the dispersion of $BaSO_4$ particles. Since a decrease in fracture toughness $K_{IC}$ of the acrylic material resulted from the addition of $BaSO_4$, then the $V(K_I)$ curve must effectively move towards the left of the $V(K_I)$ diagram, i.e. a constant-velocity crack will grow at a lower value of $K_I$ as the particle volume fraction increases.

## 4.2. Effect of glass spheres

A $V(K_I)$ diagram for the glass filled acrylic composite is shown in Fig. 6. Two principle effects

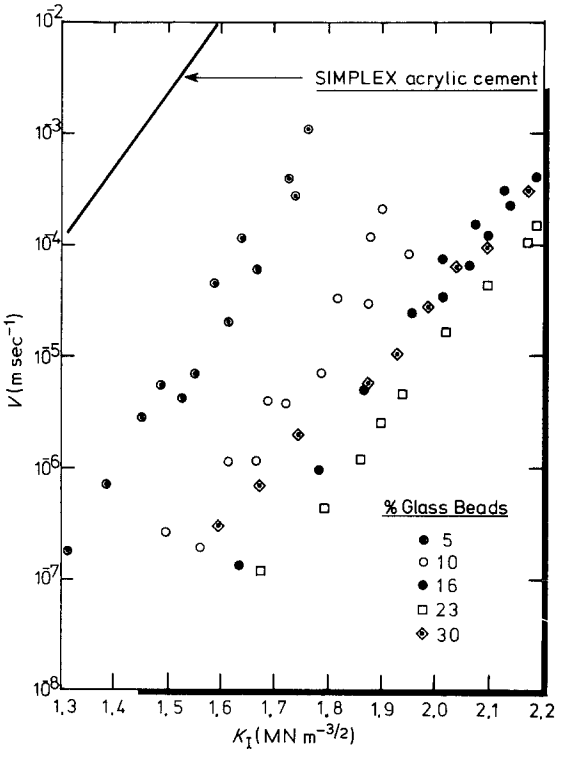


*Figure 6* Fracture surface energy $\Gamma_c$ and plane strain fracture toughness $K_{IC}$ of acrylic bone *cement* as a function of volume fraction of $BaSO_4$ dispersions.

of the glass spheres can be seen; (1) an increase in particle volume fraction $V_p$ results in a decrease in crack velocity $V$ for a given value of $K_I$ up to a critical value of $V_p$ of 0.25 approximately, and (2) at $V_p > V_{p(crit)}$, the crack velocity increases as a result of a further increase in $V_p$, for a given value of $K_I$.

The slope $n$ for each curve is essentially constant ($n = 24$) and as a result, there does not appear to be a threshold value of $K_I$ below which

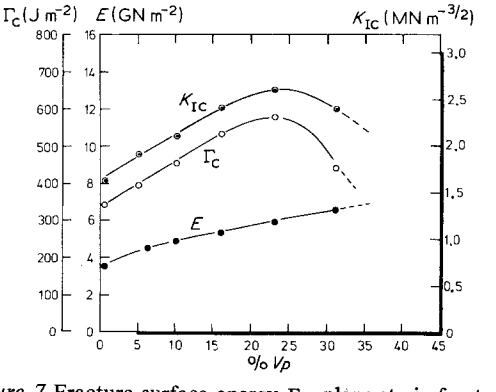


*Figure 7* Fracture surface energy $\Gamma_c$, plane strain fracture toughness $K_{IC}$ and Young's modulus $E$, of glass-filled acrylic bone *cement*. (The values were obtained in a 3-point flexural beam test).

no cracking occurs, at least over the range of $K_I$ values investigated.

Measurements of Young's modulus $E$, plane-strain fracture toughness $K_{IC}$, and fracture surface energy $\Gamma_c$, as a function of glass content are shown in Fig. 7. $E$ increases by a small amount with increasing $V_p$, whilst $K_{IC}$ and $\Gamma_c$ both reach peak values at $V_p = 0.25$ approximately. This critical value of $V_p$ is equal to $V_{p(crit)}$ determined in the subcritical crack growth study (Fig. 6). Similar peaks have been observed in fracture surface energy/particle volume fraction curves for an epoxy resin/$Al_2O_3 \cdot 3H_2O$ composite ($\bar{d} = 12\,\mu m$) [4], an epoxy resin/glass composite ($\bar{d} = 30\,\mu m$) [5] and an epoxy resin/silica composite ($\bar{d} = 70\,\mu m$) [6]. In each case, maxima occurred at a particle volume fraction of between 0.20 and 0.25.

### 4.3. Crack front–particle interaction effects

The increase in $\Gamma_c$ of the glass–acrylic composite up to $V_{p(crit)}$ (Fig. 7) may be due to crack front–particle interaction effects. Theories of particle strengthening of brittle materials emphasize the energy to create fracture surface and energy expended in increasing the length of the crack front as it bows out between 2 neighbouring obstacles [7–9]. The crack front is assumed to be pinned at each obstacle and to bow out between them, and to finally break away at a critical loop size and progress unhindered through the matrix (Fig. 8). The stress necessary to propagate a crack between an array of impenetrable obstacles, $\sigma_A$, is dependent upon the line tension effect of the crack front [9];

$$\sigma_A^2 = \frac{2E}{\pi a}\left(\Gamma_m + \frac{T}{\lambda}\right) \qquad (4)$$

where $a$ is the depth of a primary crack, $\lambda$ is the obstacle spacing, $T$ is the line energy per unit length of crack front, and $\Gamma_m$ is the fracture surface energy of the matrix. Alternatively, Equation 4 can be rewritten in terms of the fracture surface energy of the composite;

$$\Gamma_c = \Gamma_m + \frac{T}{\lambda} + \Gamma_p \qquad (5)$$

where $\Gamma_p$ takes into account any plastic work that is done on the obstacle or matrix close to the obstacle as the crack progresses. The fracture stress of the composite, $\sigma_f$, is then given by

$$\sigma_f = \left(\frac{2E\Gamma_c}{\pi a}\right) \qquad (6)$$

A prediction of the strength of the composite can be made by calculating the value of $T$ for the particular geometry of particle and particle spacing*.

When the stress necessary to link up an array of semi-elliptical micro-cracks between a regular series of obstacles is greater than the stress to propagate a single primary crack, then the fracture stress of the composite is given by Equation 4 where the value of $T$ increases as the ratio of $d/\lambda$ increases. Values of the line tension $T$ can be calculated from $\sigma_A$ in Equation 4 and have been

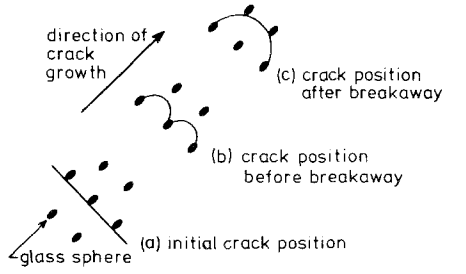


*Figure 8* A schematic representation of the interaction of a moving crack front and an array of brittle obstacles.

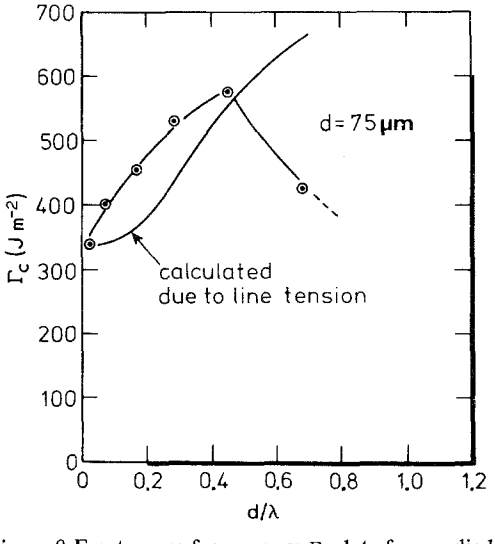


*Figure 9* Fracture surface energy $\Gamma_c$ data for acrylic bone *cement* containing a dispersion of glass spheres as a function of $d/\lambda$. The solid curve was calculated using the crack-front bowing model of Evans [9].

*The average spacing, $\lambda$, between spherical particles of equal size, $d$, can be estimated using the equation [10] $\lambda = 2d(1 - V_p)/3V_p$.

determined as a function of $d/\lambda$ and obstacle geometry [9]. A comparison between $\sigma_A$ (or $\Gamma_c$), and experimentally determined fracture strengths (or fracture surface energies) will permit an evaluation of the line tension contribution.

For small values of $d/\lambda$, (corresponding to low values of $V_p$), the data for glass spheres in acrylic *cement* falls reasonably close to the theoretical prediction of the fracture surface energy, $\Gamma_c$, containing the line tension contribution, (Fig. 9). A peak in the experimental values of $\Gamma_c$ is reached at a critical $d/\lambda$ (corresponding to $V_{p(crit)}$); for $d/\lambda < (d/\lambda)_{crit}$, the line tension contribution to $\Gamma_c$ varies with $d/\lambda$ in a similar manner to the experimentally determined variation in $\Gamma_c$, and $T$ provides a significant contribution to $\Gamma_c$.

Evans [9] has shown that the occurrence of a peak in a fracture surface energy curve of a matrix containing brittle particles probably corresponds to the onset of breakage of the particles. The fracture stress, $\sigma_A$, is given by $\epsilon_0 \sigma_A$ where $\epsilon_0$ is related to the strain-to-fracture of the obstacle. It can be thought of as an impenetrability constant, its value dependent upon $d/\lambda$. An increase in $d/\lambda$ will increase the maximum distance moved by the crack tip as it bows out to a critical loop size, and it will reduce the distance between obstacles and the line of maximum displacement between obstacles and crack tip. The result is an increase in strain in the obstacle and surrounding matrix; therefore, an increase in $d/\lambda$ will decrease the impenetrability factor $\epsilon_0$. For small values of $d/\lambda$,

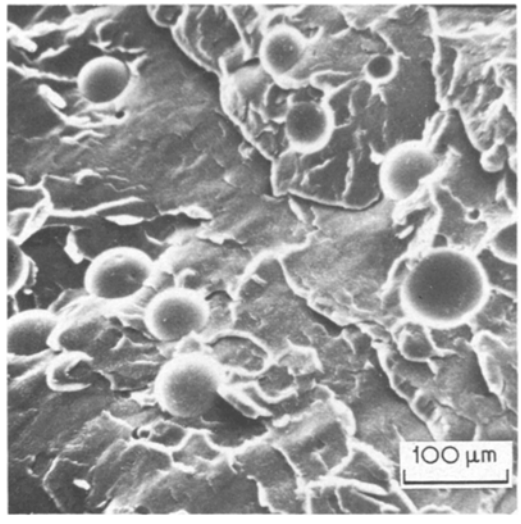


*Figure 11* Fracture surface of acrylic bone *cement* containing glass spheres ($V_p = 0.10$).

$\epsilon_0 = 1$ and the obstacles are impenetrable, but breakage may occur when $d/\lambda = (d/\lambda)_{crit}$; then $\epsilon_0$ decreases for larger $d/\lambda$. A maximum line tension $T$ contribution to $\Gamma_c$ will result at $(d/\lambda)_{crit}$; the value will depend upon the failure strains and elastic moduli of the particle and matrix.

Figs. 10–15 show typical fracture surfaces of acrylic *cements* containing either glass spheres or $BaSO_4$ particles. Bonding between glass spheres and acrylic bone *cement* is poor; this is indicated by the smooth appearance of the glass surfaces shown protruding above the fracture plain of the acrylic matrix (Figs. 11–12). No matrix could be

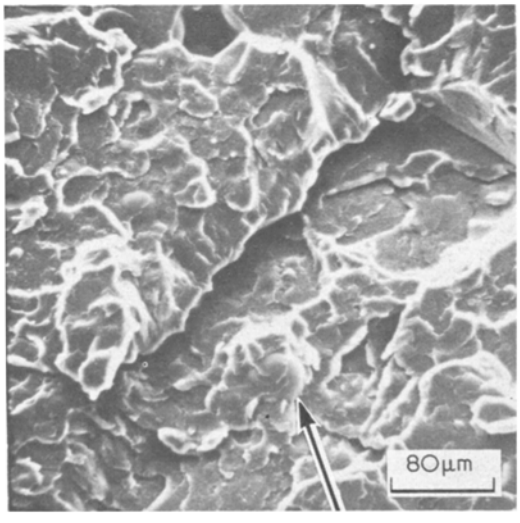


*Figure 10* Fracture surface of acrylic bone *cement*. The arrow indicates an original PMMA sphere.

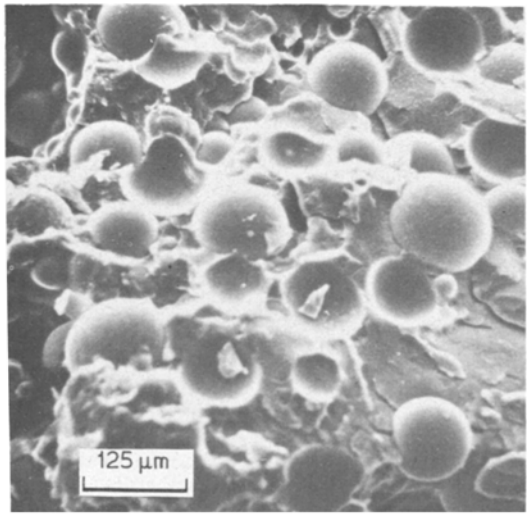


*Figure 12* Fracture surface of acrylic bone *cement* containing glass spheres ($V_p = 0.30$).

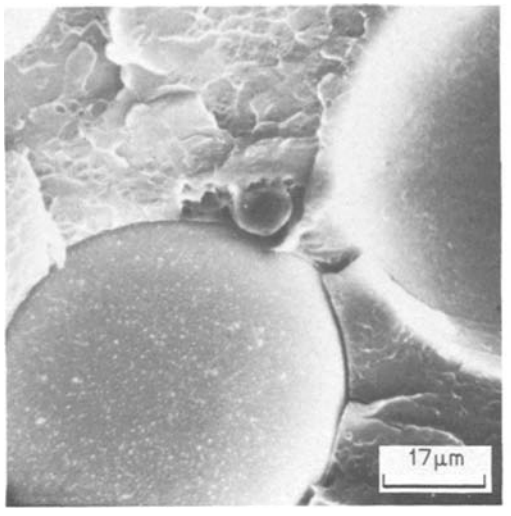


*Figure 13* Fracture surface of acrylic bone *cement* containing glass spheres ($V_p = 0.30$) showing interfacial breakdown between glass and matrix.

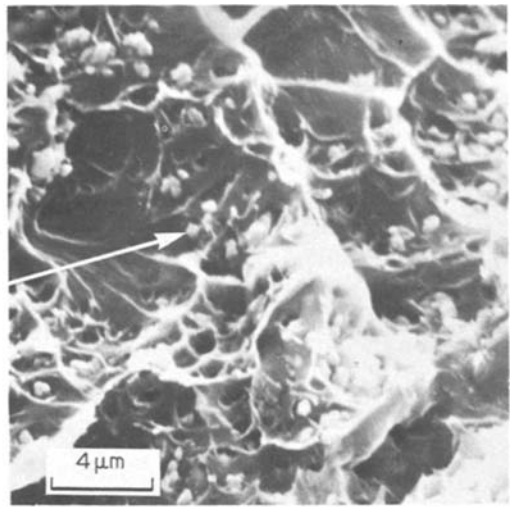


*Figure 15* Fracture surface of acrylic bone *cement* containing $BaSO_4$ ($V_p = 0.06$) showing individual particles located in voids.

seen attached to the surface of pulled-out glass spheres, and a large number of glass hemispheres beneath the fracture surface of the matrix had clearly separated from the acrylic material (Fig. 13). It did seem, however, that a greater percentage of debonded glass spheres existed in the high volume fraction composite ($V_p = 0.30$), compared to the low volume fraction composite ($V_p = 0.10$). Clearly, penetration of the glass spheres during crack propagation is not the explanation for the observed peak in the $\Gamma_c$, $d/\lambda$ curve. Perhaps, as a result of an increase in localized elastic strain energy in the particle and surrounding matrix when $d/\lambda$ increases, breakdown of the glass-acrylic bond occurs rather than breakage of the particles. The primary crack then propagates unhindered through the matrix, the glass sphere being pulled out of the matrix behind the advancing crack front, and the effect of particle–crack front interaction is lost.

In terms of the $V(K_I)$ relationship, the onset of debonding of the obstacle and passage of the crack through the matrix will result in stable cracking at lower values of $K_I$, when $d/\lambda > (d/\lambda)_{crit}$.

A decrease in $\Gamma_c$ for the $BaSO_4$/acrylic *cement* system at all values of $d/\lambda$ is due to the formation of voids around the $BaSO_4$ particles, followed by void coalescence. The coalescence occurs by elongation of the voids and tearing of the matrix between them (Figs. 14 and 15). An increase in volume fraction of $BaSO_4$ results in an increase in crack velocity (for a given value of $K_I$).

Thus, cracks will initiate at lower stresses than predicted using Equation 4, when failure of the particle–matrix bond occurs, or when voids form around particles, and they will propagate at lower values of $K_I$ without necessarily propagating catastrophically.

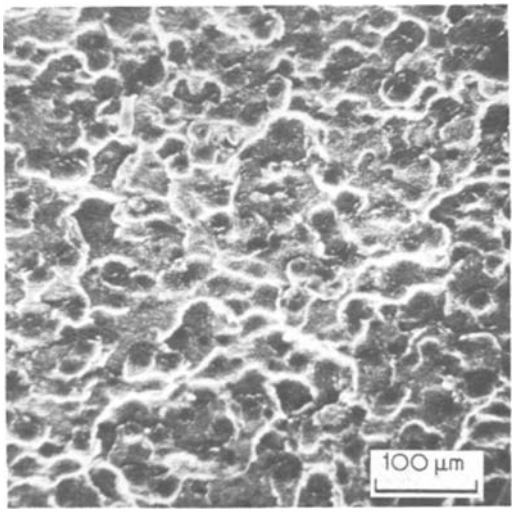


*Figure 14* Fracture surface of acrylic bone *cement* containing $BaSO_4$ particles ($V_p = 0.06$).

## 5. Conclusions and implications

The primary objective of this study was accomplished; to evaluate the effect of dispersions of barium sulphate and microscopic glass spheres upon the fracture strength and toughness of acrylic bone *cements*, and to establish crack

growth rate laws for acrylic bone *cements* in physiological environments. Slow crack growth–stress intensity factor diagrams were constructed for Simplex P acrylic *cement* composites exposed to either air, saline solution or blood serum.

As a first attempt at comparing data with theory, the data for the glass spheres/acrylic system provide some support for the crack front–line tension theory proposed by Evans. The glass spheres acted as obstacles to crack extension up to a critical particle spacing, while, in contrast, the barium sulphate particles provided no barrier whatsoever to crack propagation.

From a practical point of view, dispersions of $BaSO_4$ reduces the fracture stress and toughness and increases the rate of crack growth in static fatigue. This will have an adverse effect upon the time-to-failure of acrylic bone *cements*. In contrast, the dispersion of glass spheres increases the fracture toughness and reduces the crack growth rate by up to 3 orders of magnitude, which will have beneficial effects on the time-to-failure of the acrylic bone *cement*. Fortunately, the presence of either saline solution or blood serum has no part to play in the cracking phenomena.

## Acknowledgements

The work described in this paper forms part of a larger programme on fracture of polymers supported by the Science Research Council. We would like to thank Mr. L. Shadbolt of Howmedica Inc. for supplying us with samples of Simplex P surgical acrylic bone *cement*.

## References

1. H. AMSTUTZ, K. L. MARKOLF and G. M. McNIECE, Department of Orthopaedic Surgery, U.C.L.A. Medical School, Los Angeles; private communication 1976.
2. P. W. R. BEAUMONT and R. J. YOUNG, *J. Mater. Sci.* **10** (1975) 1334.
3. A. G. EVANS, *ibid* **7** (1972) 1137.
4. F. F. LANGE and K. C. RADFORD, *ibid* **6** (1971) 1197.
5. L. J. BROUTMAN and S. SAHU, *Mat. Sci. Eng.* **8** (1971) 98.
6. R. J. YOUNG and P. W. R. BEAUMONT, *J. Mater. Sci.* **12** (1977) 684.
7. J. FRIEDEL, "Fracture", edited by Averback *et al.* (J. Wiley, New York, 1959).
8. F. F. LANGE, *Phil. Mag.* **22** (1970) 983.
9. A. G. EVANS, *ibid* **27** (1972) 1327.
10. R. L. FULLMAN, *Trans. AIME* **197** (1953) 447.

Received 25 November 1976 and accepted 21 January 1977.